Enhancement of tripartite quantum correlation by coherent feedback control

Yinyin Zhong[1] and Jietai Jing ®[1,2,3,*]

[1]*State Key Laboratory of Precision Spectroscopy, Joint Institute of Advanced Science and Technology,*
School of Physics and Electronic Science, East China Normal University, Shanghai 200062, China
[2]*Collaborative Innovation Center of Extreme Optics, Shanxi University, Taiyuan, Shanxi 030006, China*
[3]*Department of Physics, Zhejiang University, Hangzhou 310027, China*

Measurement-free coherent feedback control is promising to manipulate various quantum optical systems for preparing nonclassical states of light. In this paper, three different coherent feedback control systems are constructed based on cascaded four-wave mixing processes. By utilizing a beam splitter as the feedback controller, we theoretically investigate the enhancement of tripartite quantum correlation and its pairwise correlation. The absorption effect of Rb vapor cells and the loss of optical propagation in the coherent feedback loop are also taken into account. The quantum correlation in the three structures can be characterized by the degree of relative intensity squeezing of the output fields. We find that the tripartite quantum correlation can be maximally enhanced by an optimal feedback ratio. In addition, two of the three pairwise correlations in the quantum regime can also be improved by tuning the strength of feedback, while the other pairwise correlation remains in the classical regime. Our results pave the way for the experimental implementation and may find potential applications in quantum communication and quantum metrology.

I. INTRODUCTION

Quantum correlation shared among multiple quantum correlated beams is important for both the fundamental science [1,2] and quantum information technology [3,4]. In recent years, four-wave mixing (FWM) processes have been experimentally demonstrated to be a successful technique to generate multiple quantum correlated beams in the hot Rb vapor cell [5–8] for its strong nonlinearity, multispatial mode nature, and natural spatial separation of the generated nonclassical beams [9]. Due to these advantages, FWM has also found a variety of interesting applications [10–23]. With the rapid development of quantum technology, a high degree of quantum correlation is of great significance, not only to improve the communication fidelity of the quantum information protocol [24–26] but also to improve the measurement precision of quantum metrology [17,27–29]. Quantum control has been investigated for a long time [30–34] and widely used in various protocols to improve the properties of systems [35–38]. Its advantages over classical approaches indicate that quantum control plays a fundamental role in emerging quantum technologies [39,40].

Quantum feedback control is an important concept in quantum control theory [41,42]. The control methods are usually divided into two types: measurement-based quantum feedback control [35,36] and coherent feedback control (CFC) [37,38,41]. The CFC scheme feeds the output field of the controlled system back into the initial inputs to manipulate the system. It has been applied to quantum error correction [43,44] and optical field squeezing enhancement by placing a linear optical component in a simple coherent feedback loop [45,46]. Because no measurement process is involved

and no back-action noise is introduced into the controlled system, the CFC scheme is promising to manipulate various quantum optical systems for preparing nonclassical states of light [45–48]. Recently, our group experimentally realized a feedback optical parametric amplifier with a single FWM process and found that the quantum correlation between the output fields can be enhanced by tuning the strength of the feedback [49]. However, such study is only limited to the case of bipartite quantum correlation. Multipartite quantum correlation is important for realizing multiuser quantum communication protocol and multiparameter quantum metrology. In this paper, we theoretically investigate the enhancement of tripartite quantum correlation and its pairwise correlation by utilizing a CFC scheme. Three different CFC structures are constructed based on cascaded FWM processes, and a tunable beam splitter (BS) is introduced as the feedback controller. The BS controller controls the feedback loop by feeding part of the output conjugate field back into one input port of the cascaded FWM system. The absorption effect of Rb vapor cells and the loss of optical propagation in the coherent feedback loop are also taken into account. Specifically, for the three structures, we find that the tripartite quantum correlation can be maximally enhanced by an optimal feedback ratio. In addition, two of the three pairwise correlations in the quantum regime can also be improved by tuning the strength of feedback, while the other pairwise correlation is always in the classical regime. Our results pave the way for the experimental implementation and may find potential applications in quantum communication and quantum metrology.

This article is organized as follows. In Sec. II, we begin with a brief description of the three CFC structures and then derive the expressions of the three output fields generated from the CFC structures. In Sec. III, we characterize the quantum correlation between the three output fields by the degree
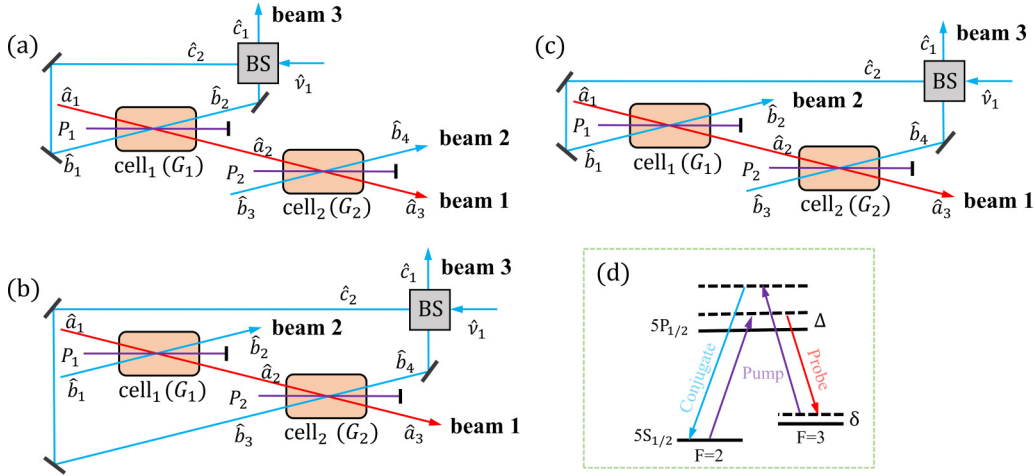
*Corresponding author: jtjing@phy.ecnu.edu.cn

FIG. 1. The theoretical models of controllable quantum feedback structures based on cascaded FWM processes. (a) $\hat{a}_1$ is the coherent input probe beam, $\hat{b}_3$ and $\hat{v}_1$ are the vacuum inputs, $\hat{a}_3$ is the amplified probe beam, and $\hat{b}_4$ and $\hat{c}_1$ are the generated conjugate beams. (b) $\hat{a}_1$ is the coherent input probe beam, $\hat{b}_1$ and $\hat{v}_1$ are the vacuum inputs, $\hat{a}_3$ is the amplified probe beam, and $\hat{b}_2$ and $\hat{c}_1$ are the generated conjugate beams. (c) $\hat{a}_1$ is the coherent input probe beam, $\hat{b}_3$ and $\hat{v}_1$ are the vacuum inputs, $\hat{a}_3$ is the amplified probe beam, and $\hat{b}_2$ and $\hat{c}_1$ are the generated conjugate beams. (d) Double-Λ scheme in the D_1 line of ^{85}Rb: Δ and δ stand for the one-photon detuning and the two-photon detuning, respectively.

of relative intensity squeezing and investigate correlation enhancement of output fields with the change of feedback ratio. The values of optimal feedback ratio are given. In Sec. IV, we study the enhancement of the pairwise correlations from the triple quantum correlated beams generated in Sec. II. In Sec. V, we give a brief conclusion of the paper.

II. CFC STRUCTURES

The conceptual models of the CFC structures based on the cascaded FWM processes are illustrated in Figs. 1(a)–1(c). For ease of expression, we named the three structures system A, system B, and system C, respectively. The graph in the green dotted frame depicts the energy-level diagram of a single FWM process in a hot Rb vapor, in which two pumped photons can convert into one probe photon and one conjugate photon, or vice versa. As shown in Fig. 1(a), a strong pump beam (P_1) and a weak coherent probe beam ($\hat{a}_1$) intersect at the center of the first hot Rb vapor cell with a slight angle. After the first FWM process, the output probe beam ($\hat{a}_2$) is amplified and a conjugate beam ($\hat{b}_2$) is generated on the other side of the pump beam simultaneously [9]. The probe beam and the conjugate beam have different frequencies. We then construct the cascaded FWM processes by taking the probe beam ($\hat{a}_2$) as the seed for the second FWM process while a pump beam (P_2) enters along the central axis of the second Rb cell. After the FWM process in the second cell, the probe beam is amplified ($\hat{a}_3$) and a new conjugate beam ($\hat{b}_4$) is generated at the same time. The input-output relationship of the two FWM processes can be expressed as

$$
\begin{aligned}
\hat{a}_2 &= \sqrt{G_1}\hat{a}_1 + \sqrt{G_1 - 1}\hat{b}_1^\dagger, \\
\hat{b}_2^\dagger &= \sqrt{G_1 - 1}\hat{a}_1 + \sqrt{G_1}\hat{b}_1^\dagger, \\
\hat{a}_3 &= \sqrt{G_2}\hat{a}_2 + \sqrt{G_2 - 1}\hat{b}_3^\dagger, \\
\hat{b}_4^\dagger &= \sqrt{G_2 - 1}\hat{a}_2 + \sqrt{G_2}\hat{b}_3^\dagger,
\end{aligned}
\tag{1}
$$

where G_1 and G_2 are the intensity gains of the first and second FWM processes, respectively. Then, we introduce a linear beam splitter to construct a controllable coherent feedback structure based on the cascaded FWM processes. As shown in the Fig. 1(a), the conjugate beam ($\hat{b}_2$) is injected into the BS, and the BS as the feedback controller controls the feedback loop by feeding the output field $\hat{c}_2$ back to the other input port of the first FWM process in the cascaded FWM system. The annihilation operator is denoted as $\hat{b}_1$. The input-output relationship of the BS can be written as

$$
\begin{aligned}
\hat{c}_1 &= \sqrt{1-k}\hat{b}_2 + \sqrt{k}\hat{v}_1, \\
\hat{c}_2 &= -\sqrt{k}\hat{b}_2 + \sqrt{1-k}\hat{v}_1, \\
\hat{b}_1 &= e^{i\phi}\hat{c}_2,
\end{aligned}
\tag{2}
$$

where k is the reflectivity of the BS controller and ϕ is the phase delay introduced by the feedback path. Similarly, as shown in Fig. 1(b), system B constructs the controllable CFC structure by injecting the conjugate beam $\hat{b}_4$ into the BS and then the output beam $\hat{c}_2$ into the other input port of the second FWM process. The annihilation operator is denoted as $\hat{b}_3$. As shown in Fig. 1(c), system C injects the conjugate beam $\hat{b}_4$ into the BS and the output beam $\hat{c}_2$ into the other input port of the first FWM process, and the annihilation operator is denoted as $\hat{b}_1$. After that, through the use of Eqs. (1) and (2), the relation between the three input fields ($\hat{a}_1$, $\hat{b}_3^\dagger$, and $\hat{v}_1^\dagger$) and three output fields ($\hat{a}_3$, $\hat{b}_4^\dagger$, and $\hat{c}_1^\dagger$) of system A can be obtained by eliminating the intermediate operators $\hat{b}_1^\dagger$, $\hat{a}_2$, $\hat{b}_2^\dagger$, and $\hat{c}_2^\dagger$. The input-output relation can be expressed as

$$
\begin{pmatrix} \hat{a}_3 \\ \hat{b}_4^\dagger \\ \hat{c}_1^\dagger \end{pmatrix} = \frac{1}{1 + e^{-i\phi}\sqrt{G_1 k}} A \begin{pmatrix} \hat{a}_1 \\ \hat{b}_3^\dagger \\ \hat{v}_1^\dagger \end{pmatrix}.
\tag{3}
$$

Similarly, we can obtain the relation between the input fields ($\hat{a}_1$, $\hat{b}_1^\dagger$, and $\hat{v}_1^\dagger$) and output fields ($\hat{a}_3$, $\hat{b}_2^\dagger$, and $\hat{c}_1^\dagger$) of

system B as

$$
\begin{pmatrix} \hat{a}_3 \\ \hat{b}_2^\dagger \\ \hat{c}_1^\dagger \end{pmatrix} = \frac{1}{1 + e^{-i\phi}\sqrt{G_2 k}} B \begin{pmatrix} \hat{a}_1 \\ \hat{b}_1^\dagger \\ \hat{v}_1^\dagger \end{pmatrix}.
\tag{4}
$$

The input-output relation of system C can also be calculated and expressed as

$$
\begin{pmatrix} \hat{a}_3 \\ \hat{b}_2^\dagger \\ \hat{c}_1^\dagger \end{pmatrix} = \frac{1}{1 + e^{-i\phi}\sqrt{(G_1 - 1)(G_2 - 1)k}} C \begin{pmatrix} \hat{a}_1 \\ \hat{b}_3^\dagger \\ \hat{v}_1^\dagger \end{pmatrix}.
\tag{5}
$$

Here,

$$
A = \begin{pmatrix} \sqrt{G_1 G_2} + e^{-i\phi}\sqrt{G_2 k} & \sqrt{G_2 - 1} + e^{-i\phi}\sqrt{G_1(G_2 - 1)k} & e^{-i\phi}\sqrt{(G_1 - 1)G_2(1 - k)} \\ \sqrt{G_1(G_2 - 1)} + e^{-i\phi}\sqrt{(G_2 - 1)k} & \sqrt{G_2} + e^{-i\phi}\sqrt{G_1 G_2 k} & e^{-i\phi}\sqrt{(G_1 - 1)(G_2 - 1)(1 - k)} \\ \sqrt{(G_1 - 1)(1 - k)} & 0 & \sqrt{k} + e^{-i\phi}\sqrt{G_1} \end{pmatrix},
\tag{6}
$$

$$
B = \begin{pmatrix} \sqrt{G_1 G_2} + e^{-i\phi}\sqrt{G_1 k} & \sqrt{(G_1 - 1)G_2} + e^{-i\phi}\sqrt{(G_1 - 1)k} & e^{-i\phi}\sqrt{(G_2 - 1)(1 - k)} \\ \sqrt{G_1 - 1} + e^{-i\phi}\sqrt{G_2(G_1 - 1)k} & \sqrt{G_1} + e^{-i\phi}\sqrt{G_1 G_2 k} & 0 \\ \sqrt{G_1(G_2 - 1)(1 - k)} & \sqrt{(G_1 - 1)(G_2 - 1)(1 - k)} & \sqrt{k} + e^{-i\phi}\sqrt{G_2} \end{pmatrix},
\tag{7}
$$

$$
C = \begin{pmatrix} \sqrt{G_1 G_2} & \sqrt{G_2 - 1} - e^{-i\phi}\sqrt{(G_1 - 1)k} & e^{-i\phi}\sqrt{(G_1 - 1)G_2(1 - k)} \\ \sqrt{G_1 - 1} - e^{-i\phi}\sqrt{(G_2 - 1)k} & -e^{-i\phi}\sqrt{G_1 G_2 k} & e^{-i\phi}\sqrt{G_1(1 - k)} \\ \sqrt{G_1(G_2 - 1)(1 - k)} & \sqrt{G_2(1 - k)} & \sqrt{k} + e^{-i\phi}\sqrt{(G_1 - 1)(G_2 - 1)} \end{pmatrix}.
\tag{8}
$$

Since there are unavoidable losses in any real experiment, we take two types of losses into consideration, namely, the FWM vapor cell's absorption effect (atomic absorption) [50,51] and the propagation loss of the light beam in the feedback loop. We model the propagation loss in the free space on the feedback path by inserting a BS shown as the gray block in Fig. 2(a), where one input is the feedback beam and the other is a vacuum state [52]. The scattering matrix is given by

$$
L = \begin{pmatrix} \sqrt{\eta} & \sqrt{1 - \eta} \\ -\sqrt{1 - \eta} & \sqrt{\eta} \end{pmatrix},
\tag{9}
$$

where η represents the optical transmission efficiency in the feedback loop due to the imperfect optical transmission. As shown in Fig. 2(b), the absorption effect in the FWM can be modeled by distributed gain and loss [50,53]. For the sake of simplicity of calculation, the loss from atomic absorption in the hot Rb vapor cell is also considered as a fictitious beam splitter introducing a vacuum state into each probe beam and conjugate beam. Therefore, for system A described in Fig. 1(a), the annihilation operators of the vacuum modes introduced by the losses are denoted as $\hat{v}_i$ ($i = 2, 3, 4, 5, 6$), and the standard beam splitter relations give

$$
\begin{aligned}
\hat{a}_2(t) &\to \sqrt{\zeta_1}\hat{a}_2 + \sqrt{1 - \zeta_1}\hat{v}_2, \\
\hat{b}_2(t) &\to \sqrt{\zeta_2}\hat{b}_2 + \sqrt{1 - \zeta_2}\hat{v}_3, \\
\hat{a}_3(t) &\to \sqrt{\zeta_3}\hat{a}_3 + \sqrt{1 - \zeta_3}\hat{v}_4, \\
\hat{b}_4(t) &\to \sqrt{\zeta_4}\hat{b}_4 + \sqrt{1 - \zeta_4}\hat{v}_5, \\
\hat{c}_2(t) &\to \sqrt{\eta}\hat{c}_2 + \sqrt{1 - \eta}\hat{v}_6,
\end{aligned}
\tag{10}
$$

where ζ_1, ζ_2, ζ_3, and ζ_4 represent the internal optical transmission efficiencies in the two Rb vapor cells for probe and conjugate fields. For simplicity, we consider all the transmission
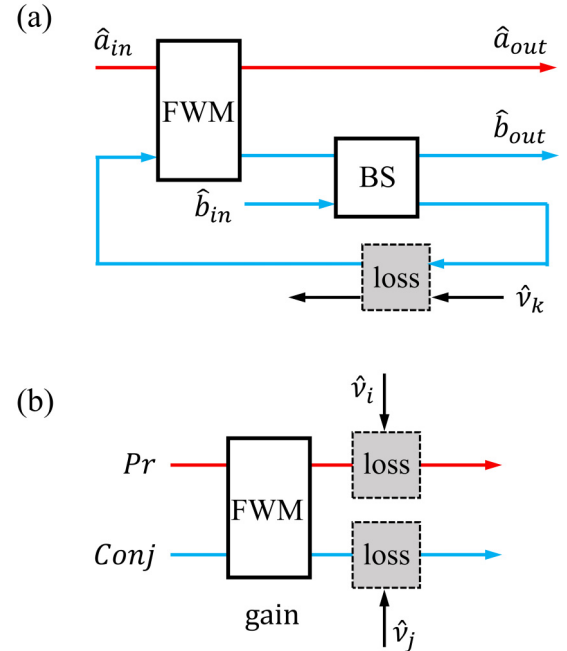

FIG. 2. (a) Model for propagation loss in the feedback loop: $\hat{v}_k$ is the vacuum mode introduced by the propagation loss. (b) The gain and loss model of the single FWM process: $\hat{v}_i$ and $\hat{v}_j$ are the vacuum modes introduced by the loss from atomic absorption in a hot Rb vapor cell. Pr, probe beam; Conj, conjugate beam.

efficiencies ζ_1, ζ_2, ζ_3, and ζ_4 in two Rb cells as ζ. Then we can easily calculate the expressions of the output fields generated from the three CFC structures followed by optical losses. After eliminating intermediate variables, by using Eqs. (1), (2), and (10), we obtain the relation between the input fields ($\hat{a}_1$, $\hat{b}_3^\dagger$, $\hat{v}_1^\dagger$, $\hat{v}_2$, $\hat{v}_3^\dagger$, $\hat{v}_4$, $\hat{v}_5^\dagger$, and $\hat{v}_6^\dagger$) and the output fields ($\hat{a}_3$, $\hat{b}_4^\dagger$, and $\hat{c}_1^\dagger$) of system A. The input-output relation can be shown as

$$
\begin{pmatrix} \hat{a}_3 \\ \hat{b}_4^\dagger \\ \hat{c}_1^\dagger \end{pmatrix} = \frac{1}{1 + e^{-i\phi}\sqrt{G_1\eta\zeta k}} \begin{pmatrix} A_{11} & A_{12} & \cdots & A_{18} \\ A_{21} & A_{22} & \cdots & A_{28} \\ A_{31} & A_{32} & \cdots & A_{38} \end{pmatrix} \begin{pmatrix} \hat{a}_1 \\ \hat{b}_3^\dagger \\ \hat{v}_1^\dagger \\ \hat{v}_2 \\ \hat{v}_3^\dagger \\ \hat{v}_4 \\ \hat{v}_5^\dagger \\ \hat{v}_6^\dagger \end{pmatrix}.
\tag{11}
$$

Similarly, for system B described in Fig. 1(b), the relation between the input fields ($\hat{a}_1$, $\hat{b}_1^\dagger$, $\hat{v}_1^\dagger$, $\hat{v}_2$, $\hat{v}_3^\dagger$, $\hat{v}_4$, $\hat{v}_5^\dagger$, and $\hat{v}_6^\dagger$) and the output fields ($\hat{a}_3$, $\hat{b}_2^\dagger$, and $\hat{c}_1^\dagger$) can be shown as

$$
\begin{pmatrix} \hat{a}_3 \\ \hat{b}_2^\dagger \\ \hat{c}_1^\dagger \end{pmatrix} = \frac{1}{1 + e^{-i\phi}\sqrt{G_2\eta\zeta k}} \begin{pmatrix} B_{11} & B_{12} & \cdots & B_{18} \\ B_{21} & B_{22} & \cdots & B_{28} \\ B_{31} & B_{32} & \cdots & B_{38} \end{pmatrix} \begin{pmatrix} \hat{a}_1 \\ \hat{b}_1^\dagger \\ \hat{v}_1^\dagger \\ \hat{v}_2 \\ \hat{v}_3^\dagger \\ \hat{v}_4 \\ \hat{v}_5^\dagger \\ \hat{v}_6^\dagger \end{pmatrix}.
\tag{12}
$$

The input-output relation of system C can also be calculated and shown as

$$
\begin{pmatrix} \hat{a}_3 \\ \hat{b}_2^\dagger \\ \hat{c}_1^\dagger \end{pmatrix} = \frac{1}{\varepsilon} \begin{pmatrix} C_{11} & C_{12} & \cdots & C_{18} \\ C_{21} & C_{22} & \cdots & C_{28} \\ C_{31} & C_{32} & \cdots & C_{38} \end{pmatrix} \begin{pmatrix} \hat{a}_1 \\ \hat{b}_3^\dagger \\ \hat{v}_1^\dagger \\ \hat{v}_2 \\ \hat{v}_3^\dagger \\ \hat{v}_4 \\ \hat{v}_5^\dagger \\ \hat{v}_6^\dagger \end{pmatrix}.
\tag{13}
$$

Here,

$$
\varepsilon = 1 + e^{-i\phi}\sqrt{(G_1-1)(G_2-1)\eta k\zeta},
\tag{14}
$$

$$
A_{11} = \sqrt{G_1 G_2}\zeta + e^{-i\phi}\sqrt{G_2\eta k}\zeta^{3/2}, \quad A_{21} = \frac{\sqrt{G_2-1}}{\sqrt{G_2}}A_{11}, \quad A_{31} = \sqrt{(G_1-1)(1-k)\zeta},
$$

$$
A_{12} = \sqrt{(G_2-1)\zeta} + e^{-i\phi}\sqrt{G_1(G_2-1)\eta k}\zeta, \quad A_{22} = \frac{\sqrt{G_2}}{\sqrt{G_2-1}}A_{12}, \quad A_{32} = 0,
$$

$$
A_{13} = e^{-i\phi}\sqrt{(G_1-1)G_2\eta(1-k)}\zeta, \quad A_{23} = \frac{\sqrt{G_2-1}}{\sqrt{G_2}}A_{13}, \quad A_{33} = \sqrt{k} + e^{-i\phi}\sqrt{G_1\eta}\zeta,
$$

$$
A_{14} = \sqrt{G_2(1-\zeta)\zeta} + e^{-i\phi}\sqrt{G_1 G_2\eta k(1-\zeta)}\zeta, \quad A_{24} = \frac{\sqrt{G_2-1}}{\sqrt{G_2}}A_{14}, \quad A_{34} = 0,
$$

$$
A_{15} = -e^{-i\phi}\sqrt{(G_1-1)G_2\eta k(1-\zeta)}\zeta, \quad A_{25} = \frac{\sqrt{G_2-1}}{\sqrt{G_2}}A_{15}, \quad A_{35} = \sqrt{(1-k)(1-\zeta)},
$$

$$
A_{16} = \sqrt{1-\zeta} + e^{-i\phi}\sqrt{G_1\eta k(1-\zeta)}\zeta, \quad A_{26} = 0, \quad A_{36} = 0,
$$

$$A_{17} = 0, \quad A_{27} = A_{16}, \quad A_{37} = 0,$$

$$A_{18} = e^{-i\phi}\sqrt{(G_1-1)G_2(1-\eta)}\zeta, \quad A_{28} = \frac{\sqrt{G_2-1}}{\sqrt{G_2}}A_{18}, \quad A_{38} = e^{-i\phi}\sqrt{G_1(1-\eta)(1-k)}\zeta, \quad (15)$$

$$B_{11} = \sqrt{G_1 G_2}\zeta + e^{-i\phi}\sqrt{G_1\eta k}\zeta^{3/2}, \quad B_{21} = \sqrt{(G_1-1)}\zeta + e^{-i\phi}\sqrt{(G_1-1)G_2\eta k}\zeta, \quad B_{31} = \sqrt{G_1(G_2-1)(1-k)}\zeta,$$

$$B_{12} = \frac{\sqrt{G_1-1}}{\sqrt{G_1}}B_{11}, \quad B_{22} = \frac{\sqrt{G_1}}{\sqrt{G_1-1}}B_{21}, \quad B_{32} = \frac{\sqrt{G_1-1}}{\sqrt{G_1}}B_{31},$$

$$B_{13} = e^{-i\phi}\sqrt{(G_2-1)\eta\zeta(1-k)}, \quad B_{23} = 0, \quad B_{33} = \sqrt{k} + e^{-i\phi}\sqrt{G_2\eta\zeta},$$

$$B_{14} = \sqrt{G_2(1-\zeta)\zeta} + e^{-i\phi}\sqrt{\eta k(1-\zeta)}\zeta, \quad B_{24} = 0, \quad B_{34} = \sqrt{(G_2-1)(1-k)(1-\zeta)}\zeta, \quad (16)$$

$$B_{15} = 0, \quad B_{25} = \sqrt{1-\zeta} + e^{-i\phi}\sqrt{G_2\eta k\zeta(1-\zeta)}, \quad B_{35} = 0,$$

$$B_{16} = B_{25}, \quad B_{26} = 0, \quad B_{36} = 0,$$

$$B_{17} = -e^{-i\phi}\sqrt{(G_2-1)\eta k\zeta(1-\zeta)}, \quad B_{27} = 0, \quad B_{37} = \sqrt{(1-k)(1-\zeta)},$$

$$B_{18} = e^{-i\phi}\sqrt{(G_2-1)(1-\eta)}\zeta, \quad B_{28} = 0, \quad B_{38} = e^{-i\phi}\sqrt{G_2(1-\eta)(1-k)}\zeta,$$

$$C_{11} = \sqrt{G_1 G_2}\zeta, \quad C_{21} = \sqrt{(G_1-1)}\zeta - e^{-i\phi}\sqrt{(G_2-1)\eta k}\zeta^{3/2}, \quad C_{31} = \sqrt{G_1(G_2-1)(1-k)}\zeta,$$

$$C_{12} = \sqrt{(G_2-1)}\zeta - e^{-i\phi}\sqrt{(G_1-1)\eta k}\zeta^{3/2}, \quad C_{22} = -e^{-i\phi}\sqrt{G_1 G_2\eta k}\zeta, \quad C_{32} = \sqrt{G_2(1-k)}\zeta,$$

$$C_{13} = e^{-i\phi}\sqrt{(G_1-1)G_2\eta(1-k)}\zeta, \quad C_{23} = e^{-i\phi}\sqrt{G_1\eta(1-k)}\zeta, \quad C_{33} = \sqrt{k} + e^{-i\phi}\sqrt{(G_1-1)(G_2-1)\eta}\zeta,$$

$$C_{14} = \sqrt{G_2(1-\zeta)\zeta}, \quad C_{24} = -e^{-i\phi}\sqrt{G_1(G_2-1)\eta k(1-\zeta)}\zeta, \quad C_{34} = \sqrt{(G_2-1)(1-k)(1-\zeta)\zeta}, \quad (17)$$

$$C_{15} = 0, \quad C_{25} = \sqrt{1-\zeta} + e^{-i\phi}\sqrt{(G_1-1)(G_2-1)\eta k(1-\zeta)}\zeta, \quad C_{35} = 0,$$

$$C_{16} = C_{25}, \quad C_{26} = 0, \quad C_{36} = 0,$$

$$C_{17} = -e^{-i\phi}\sqrt{(G_1-1)G_2\eta k(1-\zeta)}\zeta, \quad C_{27} = -e^{-i\phi}\sqrt{G_1\eta k(1-\zeta)}\zeta, \quad C_{37} = \sqrt{(1-k)(1-\zeta)},$$

$$C_{18} = e^{-i\phi}\sqrt{(G_1-1)G_2(1-\eta)}\zeta, \quad C_{28} = e^{-i\phi}\sqrt{G_1(1-\eta)}\zeta, \quad C_{38} = e^{-i\phi}\sqrt{(G_1-1)(G_2-1)(1-\eta)(1-k)}\zeta.$$

III. TRIPARTITE QUANTUM CORRELATION

In this section, we focus on the performance of the tripartite correlation potentially existing in the three CFC systems. We characterize the quantum correlation between the three output fields by the degree of relative intensity squeezing (*DS*), which is the ratio of the quantum noise of the linear combination of the photon number operators of the three output beams to the variance at the standard quantum limit (SQL). For convenience, we record the amplified probe beam of systems A, B, and C as number 1, the beam from the BS as number 3, and the remaining output conjugate beam as number 2. For example, for system A in Fig. 1(a), the annihilation operator of beam 1 corresponds to $\hat{a}_3$, the annihilation operator of beam 2 corresponds to $\hat{b}_4$, and the annihilation operator of beam 3 corresponds to $\hat{c}_1$. Accordingly, the photon number operator can be expressed as $\hat{N}_1 = \hat{a}_3^\dagger\hat{a}_3$, $\hat{N}_2 = \hat{b}_4^\dagger\hat{b}_4$, $\hat{N}_3 = \hat{c}_1^\dagger\hat{c}_1$. Therefore, the *DS* of the triple beams is given by

$$DS_{123} = 10\log_{10}\frac{\mathrm{Var}(\hat{N}_1-\hat{N}_2-\hat{N}_3)}{\mathrm{Var}(\hat{N}_1-\hat{N}_2-\hat{N}_3)_{\mathrm{SQL}}}, \quad (18)$$

where $\mathrm{Var}(\hat{N}) = \langle\hat{N}^2\rangle - \langle\hat{N}\rangle^2$ denotes the variance of $\hat{N}$, and $\mathrm{Var}(\hat{N}_1-\hat{N}_2-\hat{N}_3)_{\mathrm{SQL}} = \langle\hat{N}_1+\hat{N}_2+\hat{N}_3\rangle$. We calculate DS_{123} according to Eqs. (11)–(18) and get the relationship between DS_{123} and the feedback ratio k, phase ϕ, gains G_1 and

G_2, and transmission efficiencies ζ and η. It has been shown that there are strong quantum correlations between the three beams generated by a cascaded FWM system in hot Rb vapor cells when $G_1 G_2 > 1$, and the tripartite correlation increases as the values of G_1 and G_2 increase [5,6].

To show how the tripartite correlation is affected when the conjugate beam is fed back to the cascaded FWM system via a BS, we set the transmission efficiencies of the probe and conjugate beams ζ to 0.95 and the optical transmission efficiency in feedback loop η to 0.98. Figure 3 describes the dependence of DS_{123} on k and ϕ. For each CFC structure, we take $G_1 = G_2 = 1.5$, 2, 3, and 5, respectively. For the DS_{123} of system A, as shown in Figs. 3(a)–3(d), when $k = 0$, the values of DS_{123} are less than zero, which is consistent with the previous results of no-feedback cases [5,6]. Additionally, it can be seen that when the phase ϕ takes the value of π and k is within a suitable range, the color of all graphics is darker than that of the case with $k = 0$ (no feedback), which indicates the enhancement of the tripartite quantum correlation by CFC. However, when further increasing the value of k, we observe the disappearance of tripartite quantum correlation caused by excessive feedback. As shown in Fig. 3(a), when k is between 0.6 and 0.8, a peak of antisqueezing appears at the π phase, which is mainly due to the superstrong intensity gains induced by the giant gain feedback at the π phase. According to
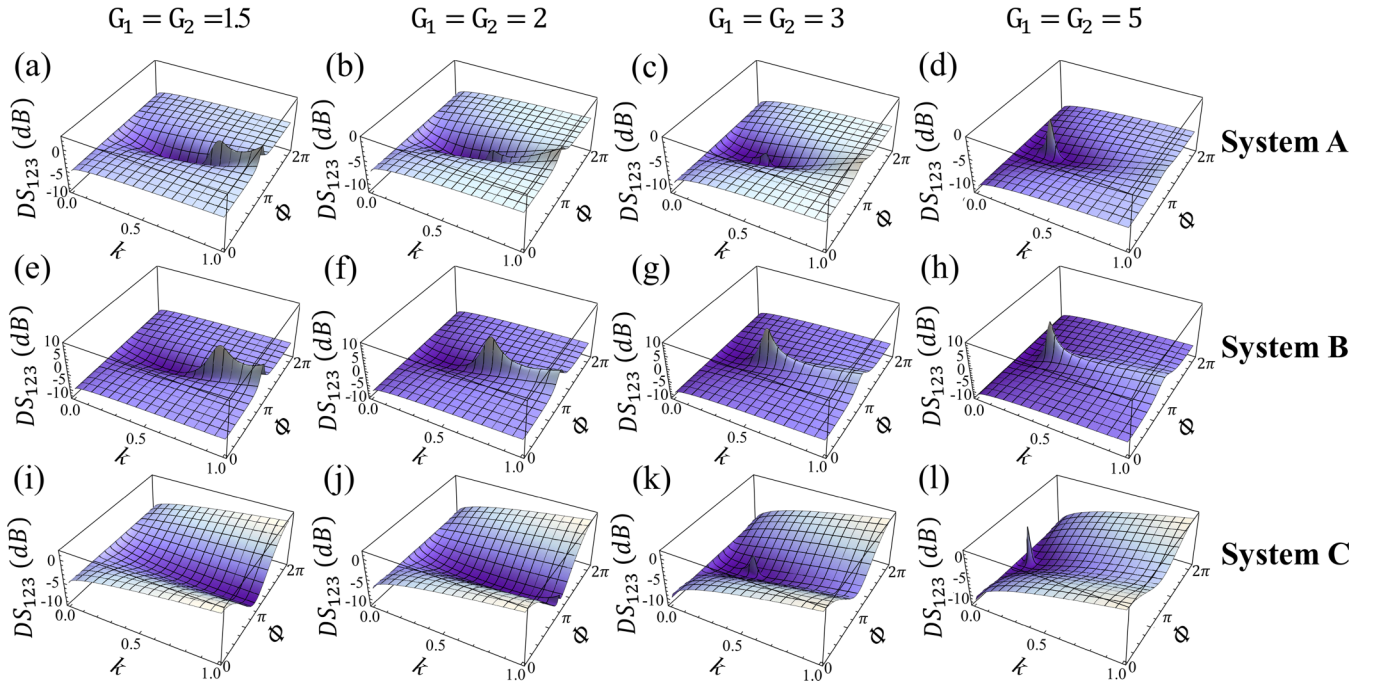
FIG. 3. The squeezing levels of $\hat{N}_1 - \hat{N}_2 - \hat{N}_3$ vary with k and ϕ when $\eta = 0.98$, $\zeta = 0.95$. System A: (a) $G_1 = G_2 = 1.5$. The squeezing level becomes maximum when $k = 0.48$ and $\phi = \pi$. (b) $G_1 = G_2 = 2$. The squeezing level becomes maximum when $k = 0.40$ and $\phi = \pi$. (c) $G_1 = G_2 = 3$. The squeezing level becomes maximum when $k = 0.17$ and $\phi = \pi$. (d) $G_1 = G_2 = 5$. The squeezing level becomes maximum when $k = 0.05$ and $\phi = \pi$. System B: (e) $G_1 = G_2 = 1.5$. The squeezing level becomes maximum when $k = 0.35$ and $\phi = \pi$. (f) $G_1 = G_2 = 2$. The squeezing level becomes maximum when $k = 0.21$ and $\phi = \pi$. (g) $G_1 = G_2 = 3$. The squeezing level becomes maximum when $k = 0.10$ and $\phi = \pi$. (h) $G_1 = G_2 = 5$. The squeezing level becomes maximum when $k = 0.04$ and $\phi = \pi$. System C: (i) $G_1 = G_2 = 1.5$. The squeezing level becomes maximum when $k = 1$ and $\phi = \pi$. (j) $G_1 = G_2 = 2$. The squeezing level becomes maximum when $k = 0.58$ and $\phi = \pi$. (k) $G_1 = G_2 = 3$. The squeezing level becomes maximum when $k = 0.11$ and $\phi = \pi$. (l) $G_1 = G_2 = 5$. The squeezing level becomes maximum when $k = 0.01$ and $\phi = \pi$.

Eq. (11), the denominators of the photon number expressions of three output beams approach zero when $k = 0.72$ with $\phi = \pi$ and $G_1 = G_2 = 1.5$, which induces the superstrong intensities of output fields. Such superstrong output intensities indicate the giant gain feedback. And the giant gain feedback leads to the vacuum noise ($\hat{v}_1$) introduced into the system being greatly amplified, which strongly deteriorates the quantum correlation of the system. When $k = 1$, all the vacuum noise from the feedback controller enters into the output field $\hat{c}_1$, and the degree of relative intensity squeezing becomes the quantum correlation between the two beams generated by such a full feedback case. The peaks in Figs. 3(b)–3(h), 3(k), and 3(l) can also be explained in the similar way as mentioned above. Besides, as shown in Figs. 3(a)–3(d), with the increase of G_1 and G_2, the range of tripartite quantum correlation shifts towards small k. This indicates that the gains of the two FWM processes can also affect the range of the disappearance of tripartite quantum correlation and change the range of k that enhances the squeezing level. For system B and system C, we can see that the quantum correlation of the three output fields can also be enhanced as shown in Figs. 3(e)–3(h) and 3(i)–3(l), respectively. Similarly, the correlation decreases by excessive feedback.

Based on the above discussions, in order to give the optimal feedback ratio k^* that maximizes the tripartite quantum correlation and compare the maximal enhancement of the tripartite quantum correlation of each system under different

gains conditions, we plot the DS_{123} within suitable feedback ratio ranges with $\phi = \pi$. The giant gain-feedback-induced peaks as mentioned above and their subsequent changes with feedback ratio are not shown in Figs. 4(a)–4(c) in order to
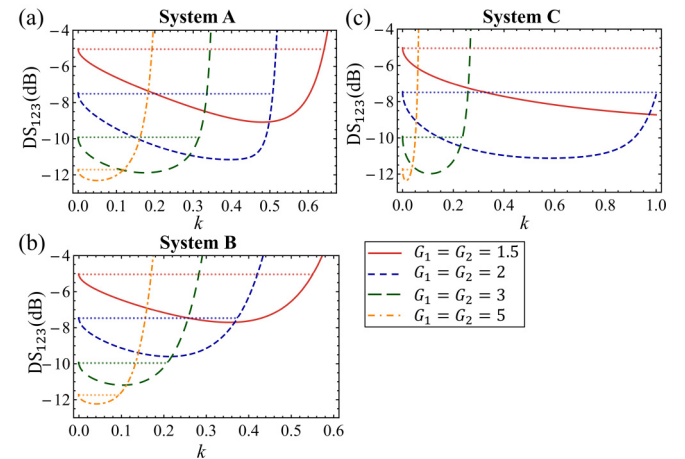

FIG. 4. The degree of relative intensity difference squeezing of the triple beams produced by (a) system A, (b) system B, and (c) system C, varying with the feedback ratio k, respectively. Here, $\eta = 0.98$ and $\zeta = 0.95$. The phase of the three systems is set to π. The dotted horizontal lines represent the value of DS_{123} when $k = 0$.

avoid confusion. As shown in Fig. 4, traces in different colors represent different values of G_1 and G_2, and the dotted horizontal lines represent the degree of relative intensity difference squeezing of the triple beams when $k = 0$ (no feedback). We can see that there always exists an optimal feedback ratio k^* to maximize the squeezing enhancement under different gain conditions. As shown in Fig. 4(a), for the DS_{123} of system A, when $G_1 = G_2 = 1.5$, 2, 3, and 5, $k^* = 0.48$, 0.40, 0.17, and 0.05, respectively. The maximal enhancement of intensity difference squeezing levels are equal to 4.0, 3.7, 2.0, and 0.6 dB, respectively. For the DS_{123} of system B which is described in Fig. 4(b), when $G_1 = G_2 = 1.5$, 2, 3, and 5, $k^* = 0.35$, 0.21, 0.10, and 0.04, respectively. The corresponding maximal enhancements of intensity difference squeezing levels are equal to 2.66, 2.13, 1.26, and 0.5 dB. For the DS_{123} of system C as shown in Fig. 4(c), when $G_1 = G_2 = 1.5$, 2, 3, and 5, $k^* = 1$, 0.58, 0.11, and 0.01, respectively. The corresponding maximal enhancements of intensity difference squeezing levels are equal to 3.69, 3.65, 2.04, and 0.64 dB. In other words, the lower the intensity gains are, the higher the squeezing enhancement will be. Here, the existence of the optimal feedback ratio can be explained by the competition between two mechanisms. The first one is the feedback mechanism that comes from the recycling of the conjugate beam on the feedback path and thus enhances the quantum properties of the three constructed systems as shown in Fig. 1. The other one is the vacuum noise mechanism that comes from the unused port of the feedback controller ($\hat{v}_1$), which deteriorates the quantum properties of the output states. The feedback mechanism dominates and the quantum correlation degradation caused by vacuum noise is not significant when k is small. Therefore, the total quantum correlation between the output fields produced by system A is increased. With further increasing of k, the effect of the vacuum noise mechanism becomes significant, and the quantum correlation is reduced. In general, when the effects of the two mechanisms balance with each other, the optimal feedback ratio is achieved and the quantum correlation enhancement is maximized. Moreover, based on the above analysis, we can see that the gains of the two FWM processes affect not only the value of the optimal feedback ratio but also the amount of enhancement of tripartite correlation.

The extra vacuum noise introduced by the losses cannot be eliminated in the real feedback control systems, which destroy the quantum property of the CFC structures. Here, we study the effect of the losses on the enhancement of tripartite quantum correlations with the constant gains for each system. As shown in Figs. 5(a)–5(c), we find that with the increasing of the values of transmission efficiencies (ζ, η), the amount of maximal enhancement of the tripartite quantum correlation induced by the CFC will increase. For the trace of $\eta = \zeta = 0.99$, which is plotted as the blue curve in Figs. 5(a)–5(c), the optimal feedback ratios $k^* = 0.42$, 0.33, and 0.71, respectively, and the corresponding enhancement of squeezing levels are equal to 8.30, 5.72, and 8.24 dB. When $\eta = 0.86$ and $\zeta = 0.83$, the value of k^* of system A is equal to 0.23, and the enhancement of squeezing level is only about 0.65 dB. The value of k^* of systems B and C are equal to 0.07 and 0.19, respectively. The corresponding enhancement of squeezing levels are equal to 0.37 and 0.70 dB, respectively.
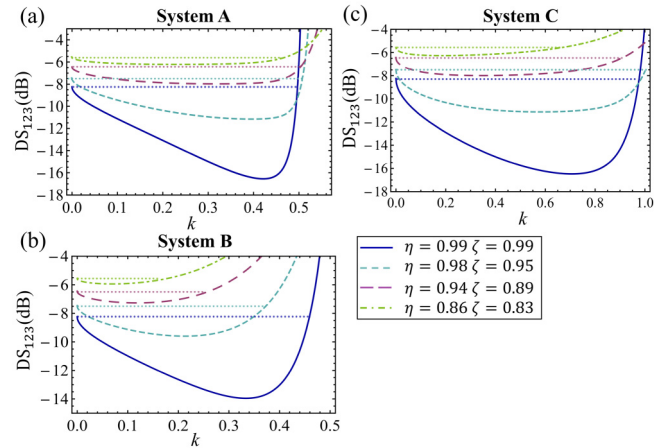

FIG. 5. The degree of relative intensity difference squeezing of the triple beams produced by (a) system A, (b) system B, and (c) system C varying with the feedback ratio k, respectively. Here, $G_1 = G_2 = 2$. The phase of the three systems is set to π.

IV. PAIRWISE CORRELATION

In this section, we study the enhancement of the pairwise correlations from the triple quantum correlated beams generated by system A, system B, and system C. The multipartite correlation shows the quantum property of the whole system while the pairwise correlations involved in the multiple quantum correlated beams provide a greatly simplified description of complex systems [54]. Therefore, the quantum correlation of any two of the multiple quantum correlated beams is also worth studying. Figure 6 depicts the quantum correlation between any two of the beams produced by the cascaded FWM system (as shown in Fig. 1) without introducing the CFC scheme. Both theoretical and experimental results [6] show that two of the three pairwise correlations can be in the quantum regime while the other pairwise correlation is always in the classical regime. Here, we study how to preserve or even enhance the quantum correlation for any bipartite group of the tripartite quantum correlated beams under the introduction of the CFC scheme. The pairwise correlations between beam i
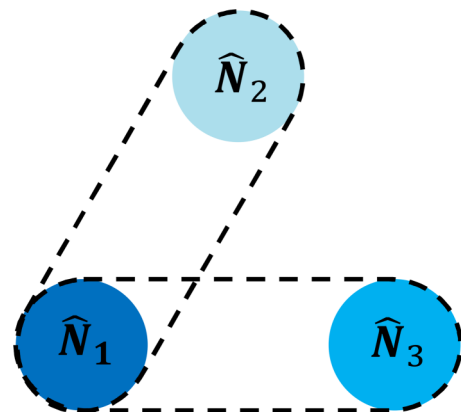

FIG. 6. The structure of pairwise correlation from triple quantum correlated beams generated by cascaded FWM processes.
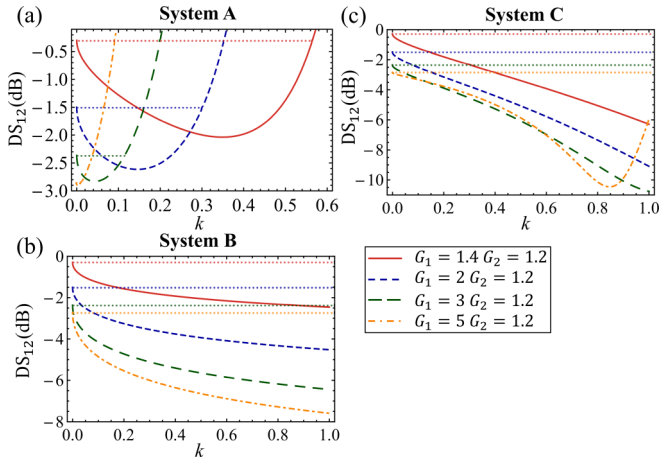
FIG. 7. The degree of relative intensity difference squeezing of beam 1 and beam 2 produced by (a) system A, (b) system B, and (c) system C varying with the feedback ratio k, respectively. Here, $\eta = 0.98$, $\zeta = 0.95$, the phase of systems A and C is set to π, and the phase of system B is set to 2π.
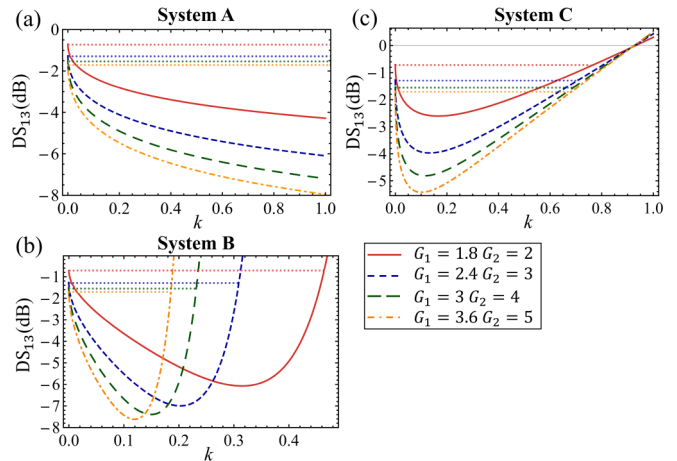

FIG. 8. The degree of relative intensity difference squeezing of beams 1 and 3 produced by (a) system A, (b) system B, and (c) system C varying with the feedback ratio k, respectively. Here, $\eta = 0.98$, $\zeta = 0.95$, the phase of system A and system C is set to 2π, and the phase of system B is set to π.

and beam j ($i, j = 1, 2, 3$ and $i \neq j$) can be quantified by

$$DS_{12} = 10 \log_{10} \frac{\text{Var}(\hat{N}_1 - \hat{N}_2)}{\text{Var}(\hat{N}_1 - \hat{N}_2)_{\text{SQL}}},$$

$$DS_{13} = 10 \log_{10} \frac{\text{Var}(\hat{N}_1 - \hat{N}_3)}{\text{Var}(\hat{N}_1 - \hat{N}_3)_{\text{SQL}}}, \qquad (19)$$

$$DS_{23} = 10 \log_{10} \frac{\text{Var}(\hat{N}_2 - \hat{N}_3)}{\text{Var}(\hat{N}_2 - \hat{N}_3)_{\text{SQL}}}.$$

We can calculate DS_{ij} by Eqs. (11)–(17) and Eq. (19). When DS_{ij} is negative and decreases as the change of feedback ratio k, we could claim that the pairwise quantum correlation exists and can be enhanced by the CFC scheme.

We plot DS_{12} versus feedback ratio k as shown in Fig. 7. It should be noted that for each system, we take the appropriate phase value to maximize the squeezing degree. We take the value of G_2 of the three systems as 1.2. Figures 7(a)–7(c) show that the value of DS_{12} of systems A, B, and C vary with k, respectively. When $k = 0$, it corresponds to the cascaded FWM processes without feedback. We can see that the quantum correlation between beam 1 and beam 2 produced by the three systems exists. Moreover, for each trace, there always exists an optimal feedback ratio k^* to maximize the squeezing enhancement. As shown in Fig. 7(a), we can see that the quantum correlation between beam 1 and beam 2 can be further enhanced when G_1 is smaller. When $G_1 = 1.4$, 2, and 3, $k^* = 0.35$, 0.15, and 0.04, respectively. The corresponding maximal enhancements of intensity difference squeezing levels are about 1.7, 1.12, and 0.46 dB. When $G_1 = 5$, k^* is close to zero, and the corresponding maximal squeezing enhancement is only about 0.03 dB. And then the pairwise correlation between beam 1 and beam 2 decreases with further increase of feedback ratio k due to the excessive feedback. The DS_{12} of system B versus feedback ratio k is shown in Fig. 7(b). We can see that the squeezing enhancement reaches its

maximum at $k = 1$. When $G_1 = 1.4$, the maximal enhancement of squeezing level is about 2.16 dB. When $G_1 = 5$, the maximal enhancement is about 5.5 dB. As shown in Fig. 7(c), for values of G_1 from 1.4 to 3, the squeezing enhancement of system C reaches the maximum at $k = 1$, and the corresponding maximal enhancements of squeezing levels are equal to 6.0, 7.6, and 8.4 dB. However, when $G_1 = 5$, the optimal feedback ratio k^* is equal to 0.85, and the enhancement of the pairwise correlation between beam 1 and beam 2 produced by system C decreases by excessive feedback. The corresponding maximal enhancement of squeezing level is about 7.6 dB.

As shown in Fig. 8, the quantum correlation between beam 1 and beam 3 exists and can also be enhanced by varying the value of k. For the DS_{13} of system A as shown in Fig. 8(a), when $G_1 = 1.8$ and $G_2 = 2$, the optimal feedback ratio k^* to maximize the squeezing enhancement is equal to 1 and the corresponding value of DS_{13} is -4.3 dB; about 3.6 dB enhancement of the squeezing level is obtained. When $G_1 = 3.6$ and $G_2 = 5$, $k^* = 1$ and the corresponding value of DS_{13} is -8 dB; about 6.3 dB enhancement of the squeezing level is obtained. For the DS_{13} of system B, as shown in Fig. 8(b), when $G_1 = 1.8$ and $G_2 = 2$, $k^* = 0.31$ and the corresponding DS_{13} is -6.08 dB; about 5.4 dB enhancement of the squeezing level is obtained. When $G_1 = 3.6$ and $G_2 = 5$, $k^* = 0.12$ and the corresponding DS_{13} is -7.6 dB; about 5.9 dB enhancement of the squeezing level is obtained. For the DS_{13} of system C as shown in Fig. 8(c), when $G_1 = 1.8$ and $G_2 = 2$, $k^* = 0.17$ and the corresponding value of DS_{13} is -2.6 dB; about 1.9 dB enhancement of the squeezing level is obtained. When $G_1 = 3.6$ and $G_2 = 5$, $k^* = 0.10$ and the corresponding value of DS_{13} is -5.4 dB; about 3.7 dB enhancement of the squeezing level is obtained. As shown in Fig. 9, the DS_{23} of the three systems is always positive, meaning that the pairwise correlation between beam 2 and beam 3 is always in the classical regime. This is consistent with the theoretical predictions in Fig. 6.
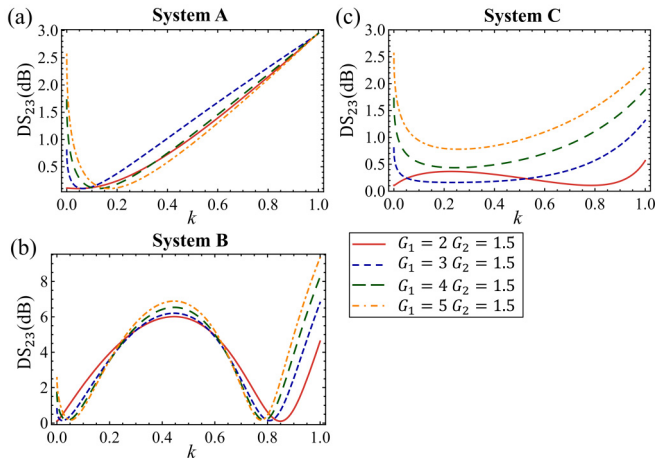
FIG. 9. The degree of relative intensity difference squeezing of beams 2 and 3 produced by (a) system A, (b) system B, and (c) system C varying with the feedback ratio k, respectively. Here, $\eta = 0.98$, $\zeta = 0.95$, the phase of system A is set to 2π, the phase of system B is set to 1.11π, and the phase of system C is set to 0.08π.

V. CONCLUSION

In this paper, we have theoretically constructed three CFC structures and each structure consists of a cascaded FWM system and a BS as the controller. We find that the tripartite correlation and two of the three pairwise correlations in the quantum regime can be enhanced by tuning the strength of the feedback. The other pairwise correlation is always in the classical regime. Moreover, we find the optimal feedback ratios that maximize the quantum correlation enhancement for both tripartite correlation and pairwise correlations. Our results show that the maximal quantum correlation enhancement is also affected by the losses in the system and the intensity gains of the two FWM processes. Our work paves the way for the implementation of the enhancement of tripartite quantum correlation by using the strategy of CFC.

[1] A. Einstein, B. Podolsky, and N. Rosen, Phys. Rev. **47**, 777 (1935).

[2] D. M. Greenberger, M. A. Horne, and A. Zeilinger, Phys. Today **46**(8), 22 (1993).

[3] H. J. Kimble, Nature (London) **453**, 1023 (2008).

[4] C. Weedbrook, S. Pirandola, R. García-Patrón, N. J. Cerf, T. C. Ralph, J. H. Shapiro, and S. Lloyd, Rev. Mod. Phys. **84**, 621 (2012).

[5] Z. Qin, L. Cao, H. Wang, A. M. Marino, W. Zhang, and J. Jing, Phys. Rev. Lett. **113**, 023602 (2014).

[6] W. Wang, L. Cao, Y. Lou, J. Du, and J. Jing, Appl. Phys. Lett. **112**, 034101 (2018).

[7] L. Cao, J. Qi, J. Du, and J. Jing, Phys. Rev. A **95**, 023803 (2017).

[8] S. Liu, H. Wang, and J. Jing, Phys. Rev. A **97**, 043846 (2018).

[9] C. F. McCormick, V. Boyer, E. Arimondo, and P. D. Lett, Opt. Lett. **32**, 178 (2007).

[10] J. Kong, J. Jing, H. Wang, F. Hudelist, C. Liu, and W. Zhang, Appl. Phys. Lett. **102**, 011130 (2013).

[11] A. MacRae, T. Brannan, R. Achal, and A. I. Lvovsky, Phys. Rev. Lett. **109**, 033601 (2012).

[12] Y. Cai, J. Feng, H. Wang, G. Ferrini, X. Xu, J. Jing, and N. Treps, Phys. Rev. A **91**, 013843 (2015).

[13] A. M. Marino, R. C. Pooser, V. Boyer, and P. D. Lett, Nature (London) **457**, 859 (2009).

[14] V. Boyer, A. M. Marino, R. C. Pooser, and P. D. Lett, Science **321**, 544 (2008).

[15] C. S. Embrey, M. T. Turnbull, P. G. Petrov, and V. Boyer, Phys. Rev. X **5**, 031004 (2015).

[16] J. Jing, C. Liu, Z. Zhou, Z. Y. Ou, and W. Zhang, Appl. Phys. Lett. **99**, 011110 (2011).

[17] R. C. Pooser and B. Lawrie, Optica **2**, 393 (2015).

[18] M. W. Holtfrerich and A. M. Marino, Phys. Rev. A **93**, 063821 (2016).

[19] A. Kumar, H. Nunley, and A. M. Marino, Phys. Rev. A **95**, 053849 (2017).

[20] R. C. Pooser and B. Lawrie, ACS Photonics **3**, 8 (2016).

[21] J. D. Swaim, E. M. Knutson, O. Danaci, and R. T. Glasser, Opt. Lett. **43**, 2716 (2018).

[22] S. Liu, Y. Lou, and J. Jing, Phys. Rev. Lett. **123**, 113602 (2019).

[23] S. Liu, Y. Lou, J. Xin, and J. Jing, Phys. Rev. Appl. **10**, 064046 (2018).

[24] S. L. Braunstein and P. van Loock, Rev. Mod. Phys. **77**, 513 (2005).

[25] A. Furusawa, J. L. Sørensen, S. L. Braunstein, C. A. Fuchs, H. J. Kimble, and E. S. Polzik, Science **282**, 706 (1998).

[26] H. Yonezawa, T. Aoki, and A. Furusawa, Nature (London) **431**, 430 (2004).

[27] B. E. Anderson, B. L. Schmittberger, P. Gupta, K. M. Jones, and P. D. Lett, Phys. Rev. A **95**, 063843 (2017).

[28] F. Hudelist, J. Kong, C. Liu, J. Jing, Z. Y. Ou, and W. Zhang, Nat. Commun. **5**, 3049 (2014).

[29] N. Otterstrom, R. C. Pooser, and B. J. Lawrie, Opt. Lett. **39**, 6533 (2014)

[30] D. Vitali, P. Tombesi, and G. J. Milburn, J. Mod. Opt. **44**, 2033 (1997).

[31] D. B. Horoshko and S. Y. Kilin, J. Mod. Opt. **44**, 2043 (1997).

[32] A. G. Butkovskiy and Yu. I. Samoilenko, *Control of Quantum-Mechanical Processes and Systems*, translated by M. B. Burov (Kluwer Academic, Dordrecht, 1990).

[33] H. M. Wiseman and G. J. Milburn, Phys. Rev. Lett. **70**, 548 (1993); Phys. Rev. A **49**, 1350 (1994).

[34] M. Keller and G. Mahler, J. Mod. Opt. **41**, 2537 (1994).

[35] C. Sayrin *et al.*, Nature (London) **477**, 73 (2011).

[36] R. Inoue, S.-I.-R. Tanaka, R. Namiki, T. Sagawa, and Y. Takahashi, Phys. Rev. Lett. **110**, 163602 (2013).

[37] H. M. Wiseman and G. J. Milburn, Phys. Rev. A **49**, 4110 (1994).

[38] R. J. Nelson, Y. Weinstein, D. Cory, and S. Lloyd, Phys. Rev. Lett. **85**, 3045 (2000).

[39] H. Mabuchi and N. Khaneja, Int. J. Robust Nonlin. Contr. **15**, 647 (2005).

[40] J. P. Dowling and G. J. Milburn, Philos. Trans. R. Soc. London A **361**, 1809 (2003).

[41] S. Lloyd, Phys. Rev. A **62**, 022108 (2000).

[42] H. M. Wiseman and G. J. Milburn, *Quantum Measurement and Control* (Cambridge University Press, Cambridge, UK, 2010).

[43] J. Kerckhoff, H. I. Nurdin, D. S. Pavlichin, and H. Mabuchi, Phys. Rev. Lett. **105**, 040502 (2010).

[44] J. Kerckhoff, D. S. Pavlichin, H. Chalabi, and H. Mabuchi, New J. Phys. **13**, 055022 (2011).

[45] J. E. Gough and S. Wildfeuer, Phys. Rev. A **80**, 042107 (2009).

[46] S. Iida, M. Yukawa, H. Yonezawa, N. Yamamoto, and A. Furasawa, IEEE Trans. Autom. Control **57**, 2045 (2012).

[47] M. Yanagisawa and H. Kimura, IEEE Trans. Autom. Control **48**, 2121 (2003).

[48] Z. Yan, X. Jia, C. Xie, and K. Peng, Phys. Rev. A **84**, 062304 (2011).

[49] X. Pan, H. Chen, T. Wei, J. Zhang, A. M. Marino, N. Treps, R. T. Glasser, and J. Jing, Phys. Rev. B **97**, 161115(R) (2018).

[50] M. Jasperse, L. D. Turner, and R. E. Scholten, Opt. Express **19**, 3765 (2011).

[51] M. Fox, *Quantum Optics: An Introduction* (Oxford University Press, New York, 2006).

[52] H. M. Wiseman, S. J. Jones, and A. C. Doherty, Phys. Rev. Lett. **98**, 140402 (2007).

[53] C. F. McCormick, A. M. Marino, V. Boyer, and P. D. Lett, Phys. Rev. A **78**, 043816 (2008).

[54] E. Schneidman, S. Still, M. J. Berry II, and W. Bialek, Phys. Rev. Lett. **91**, 238701 (2003).